Superfolder mTurquoise2ox optimized for the bacterial periplasm allows high efficiency in vivo FRET of cell division antibiotic targets

Meiresonne, N.Y.; Consoli, E.; Mertens, L.M.Y.; Chertkova, A.O.; Goedhart, J.; den Blaauwen, T.

DOI
10.1111/mmi.14206

Publication date
2019

Document Version
Final published version

Published in
Molecular Microbiology

Molecular Microbiology (2019) 111(4), 1025–1038
doi:10.1111/mmi.14206
First published online 28 February 2019

Superfolder mTurquoise2^{ox} optimized for the bacterial periplasm allows high efficiency *in vivo* FRET of cell division antibiotic targets

Nils Y. Meiresonne,[1] Elisa Consoli,[1†] Laureen M.Y. Mertens,[1†] Anna O. Chertkova,[2] Joachim Goedhart[2] and Tanneke den Blaauwen[1*]

[1] *Bacterial Cell Biology & Physiology, Swammerdam Institute for Life Sciences, University of Amsterdam, Science Park 904, Amsterdam, 1098 XH, The Netherlands.*

[2] *Molecular Cytology and van Leeuwenhoek Centre for Advanced Microscopy, Swammerdam Institute for Life Sciences, University of Amsterdam, Science Park 904, Amsterdam, 1098 XH, The Netherlands.*

Summary

Fluorescent proteins (FPs) are of vital importance to biomedical research. Many of the currently available fluorescent proteins do not fluoresce when expressed in non-native environments, such as the bacterial periplasm. This strongly limits the options for applications that employ multiple FPs, such as multiplex imaging and Förster resonance energy transfer (FRET). To address this issue, we have engineered a new cyan fluorescent protein based on mTurquoise2 (mTq2). The new variant is dubbed superfolder turquoise2ox (sfTq2^{ox}) and is able to withstand challenging, oxidizing environments. sfTq2^{ox} has improved folding capabilities and can be expressed in the periplasm at higher concentrations without toxicity. This was tied to the replacement of native cysteines that may otherwise form promiscuous disulfide bonds. The improved sfTq2^{ox} has the same spectroscopic properties as mTq2, that is, high fluorescence lifetime and quantum yield. The sfTq2^{ox}-mNeongreen FRET pair allows the detection of periplasmic protein-protein interactions with energy transfer rates exceeding 40%. Employing the new FRET pair, we show the direct interaction of two essential periplasmic cell division proteins FtsL and FtsB and disrupt it by mutations, paving the way for *in vivo* antibiotic screening.

Accepted 9 January, 2019. *For correspondence. E-mail t.denblaauwen@uva.nl; Tel. 31205253852.†The authors contributed equally.

Significance: The periplasmic space of Gram-negative bacteria contains many regulatory, transport and cell wall-maintaining proteins. A preferred method to investigate these proteins *in vivo* is by the detection of fluorescent protein fusions. This is challenging since most fluorescent proteins do not fluoresce in the oxidative environment of the periplasm. We assayed popular fluorescent proteins for periplasmic functionality and describe key factors responsible for periplasmic fluorescence. Using this knowledge, we engineered superfolder mTurquoise2ox (sfTq2^{ox}), a new cyan fluorescent protein, capable of bright fluorescence in the periplasm. We show that our improvements come without a trade-off from its parent mTurquoise2. Employing sfTq2^{ox} as FRET donor, we show the direct *in vivo* interaction and disruption of unique periplasmic antibiotic targets FtsB and FtsL.

Introduction

In Gram-negative bacteria, the cytoplasm is enveloped by an inner membrane (IM) and an asymmetric outer membrane (OM). The space between the IM and OM is called the periplasm and contains the protective peptidoglycan layer. As much as 30% of *Escherichia coli*'s proteins are predicted to localize to the envelope and many essential processes function fully or partly within the periplasm (Weiner and Li, 2008). The protein interactions in the periplasm are of great interest for biotechnological and medical purposes like synthesis of exogenous proteins and antibiotic development (Harvey *et al.*, 2004). The most direct way to observe these proteins in living cells is by fluorescence microscopy of genetically encoded fusions to fluorescent proteins (FPs). Fluorescence also provides a means of detecting protein-protein interactions by Förster resonance energy transfer (FRET). The stringent distance dependence for FRET is ideal to detect direct protein-protein interactions as these also occur in the nanometre range, whereas indirect protein interactions usually occur on a larger distance scale and are not detectable by FRET (Piston and Kremers, 2007).

In vivo studies of proteins in the periplasm are challenging because of its oxidizing environment and toxicity associated with protein over-expression (Meiresonne *et al*., 2017). Expression of FPs in the periplasm does not always result in fluorescence and only a limited number of FPs have been shown to fold and mature under periplasmic conditions. Recently, we observed good expression of mNeongreen (mNG) and used it as a donor to the mCherry (mCh) acceptor FP in an *in vivo* periplasmic FRET assay (Meiresonne *et al*., 2017). The mNG-mCh FRET pair has an R_0 of 5.5 nm (the distance at which 50% FRET occurs) and allowed the detection of periplasmic protein-protein interactions with a dynamic range of up to 16% energy transfer efficiency. However, this is only half the range of what can be achieved for cytoplasmic FRET pairs.

To improve our periplasmic FRET assay, popular existing FPs were screened for periplasmic fluorescence but none was adequate. Therefore, we rationally designed a novel FP (dubbed sfTq2) and further optimized it for periplasmic functionality creating sfTq2^{ox}. This process revealed the factors important for periplasmic fluorescence. sfTq2^{ox} has biophysical properties equal to its parent FP mTq2. Expressing it in the periplasm comes at greatly reduced toxicity, resulting in bright cyan fluorescence. sfTq2^{ox} forms a FRET pair with mNG with an R_0 of 6.0 nm and allows exceptionally high rates of energy transfer in the cytoplasm and periplasm of *E. coli*. Employing our new assay, we show the periplasmic interaction of the essential cell division proteins FtsB and FtsL. This work breaks ground for new research and provides microbiologists with new tools to use fluorescent techniques in the periplasm.

Results

Robust folding is the first prerequisite for periplasmic FP fluorescence

To optimize our periplasmic mNG-mCh FRET assay (Meiresonne *et al*., 2017), a higher R_0 value FRET pair was sought for. This could be achieved by finding an acceptor FP with high extinction coefficient and/or high spectral overlap with the mNG donor to replace mCherry. However, most FPs do not fluoresce in the Gram-negative periplasm due to hampered folding of their ß-barrel or maturation defects. These challenges are still insufficiently understood. FPs evolved to function in the eukaryotic cytoplasm and are not adapted to foreign environments. Especially challenging are compartments where protein folding occurs after translocation across a membrane as is the case for the eukaryotic endoplasmic reticulum (ER) and the bacterial periplasm. These are oxidative environments and cysteines may form promiscuous disulfide bridges resulting in non-fluorescent oligomers (Costantini *et al*., 2015). The *Anthozoa*-derived mFruits and mScarlets were thought to be good candidate acceptor FPs because of their lack of native cysteines and favourable spectroscopic properties to form a FRET pair with the established periplasmic FP mNG instead of mCherry (Table S1). The FPs were expressed in the periplasm of *E. coli* by co-translational translocation through the sec-translocase (Fig. 1).

Periplasmic FP fusions were tested for expression-related toxicity by growing *E. coli* in a plate reader in rich medium at 37°C and inducing expression at a concentration range of isopropyl-ß-D-thiogalactopyranoside (IPTG) while monitoring growth and fluorescence. All periplasmic FP constructs resulted in toxicity-associated growth curves correlating with the level of induction (Fig. S1a). Expression of cysteine-less FPs seemed less toxic compared to sfGFP and mNG. Cultures that grew relatively unimpaired produced fluorescent signals over time, which were confirmed to be periplasmic by fluorescence microscopy (Fig. S1B and C). However, expressing the same constructs for two mass doubling times at non-toxic concentrations did not result in all-round periplasmic fluorescence for living, fixed or fixed and matured samples. Of the tested mFruits, only mCherry was able to fluoresce

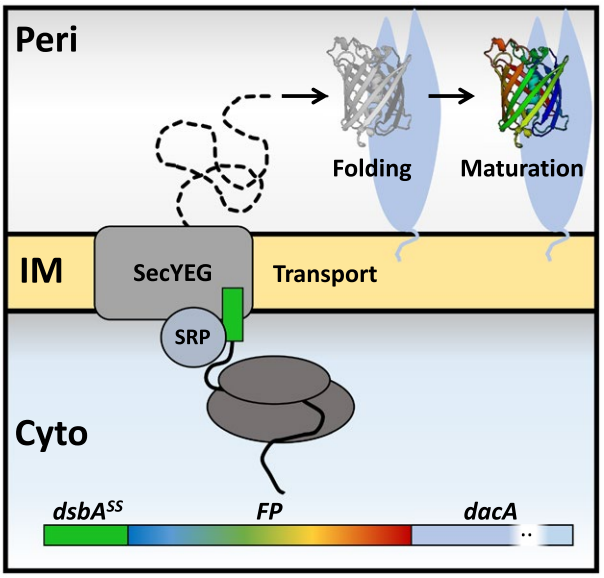

Fig. 1. Co-translational expression of FPs in the periplasm. FP fusions were expressed in the periplasm and attached to the periplasmic (Peri) side of the inner membrane (IM) through PBP5 (encoded by *dacA)*. The DsbA (*dsba*^{ss}) signal sequence is a substrate for the signal recognition particle (SRP) that directs co-translational transport through the SecYEG translocase of the N-terminal fused gene product translated in the cytoplasm (Cyto). The FP fusion is translocated to the periplasm and the signal sequence is cleaved off. Here the FP is exposed to periplasmic conditions under which it needs to efficiently fold its ß-barrel and subsequently mature its chromophore to become fluorescent. FPs that are unable to fluoresce in the periplasm thus have problems with either folding or chromophore maturation.

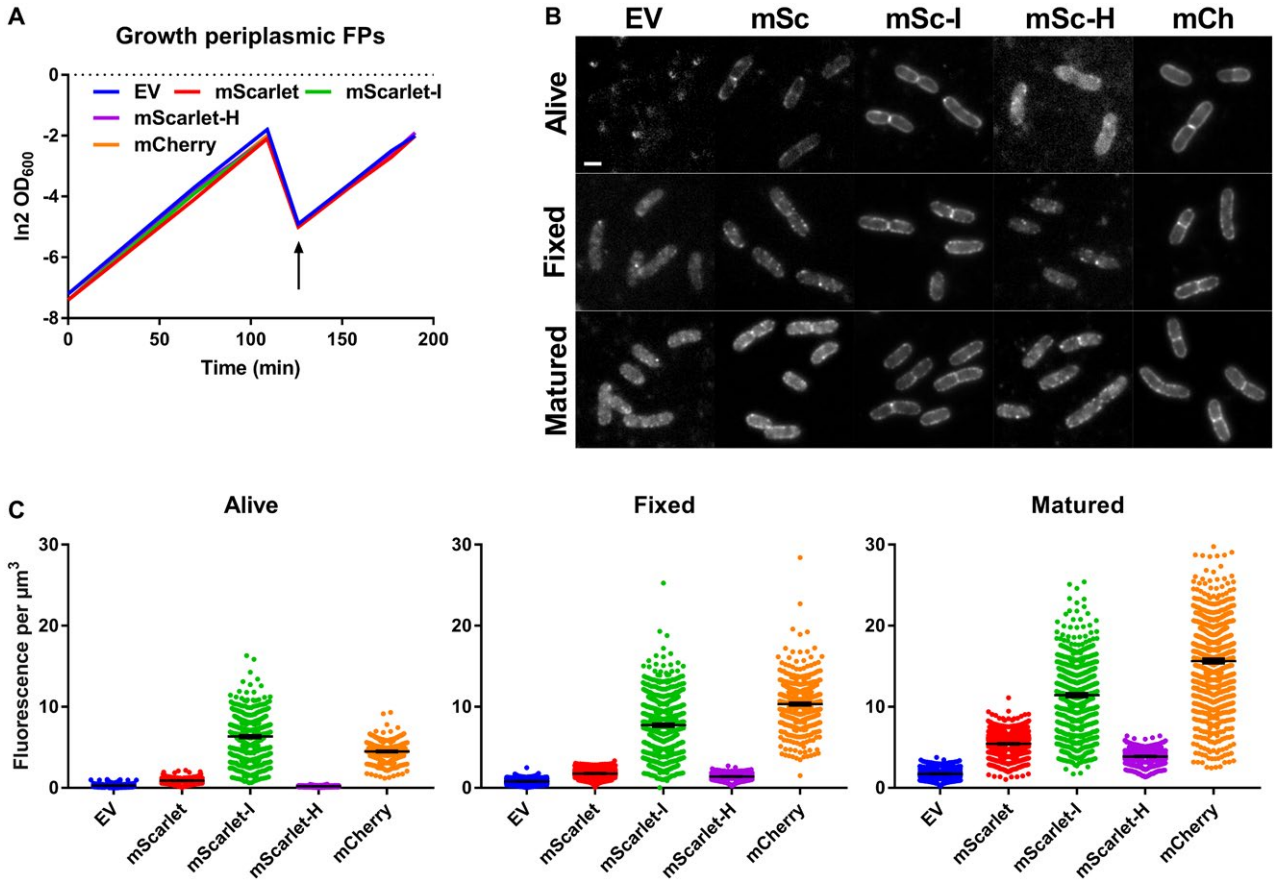

Fig. 2. mCherry is the preferred red FP in the periplasm.
A. LMC500 carrying DsbA^{ss}-FP-PBP5 plasmids for the periplasmic expression of the mScarlet FPs and mCh were grown as flask cultures in TY at 37°C and induced with 15 µM IPTG (arrow). Induction did not alter growth rates compared to a control carrying an empty plasmid (EV).
B. Fluorescence images of living, fixed and fixed and matured cells showed varying levels of periplasmic fluorescence. Note that the greyscales were set for automatically visualizing any signal. The scale bar represents 2 µm.
C. Quantification of fluorescence signals from all samples revealing strong periplasmic signals for mSc-I and mCherry. The respective number of cells analysed for the living, fixed or fixed and matured samples were: EV 415, 928 and 689, mSc 623, 868 and 1165, mSc-I 672, 1009 and 952, mSc-H 618, 569 and 758 and mCh 477, 792 and 1144. The error bars at the mean indicate the 95% confidence interval.

in the periplasm where the others only showed faint and grainy fluorescence of near background intensity (Fig. S2). The mScarlets performed better and mScarlet-I showed fluorescence in living, fixed or fixed and matured cells. mScarlet and mScarlet-H resulted in clearer periplasmic signals only after maturation. Yet, mCherry outperformed the mScarlets with brighter initial periplasmic fluorescence (Fig. 2).

Given the modest brightness of mCherry compared to the other mFruits and mScarlets, it is likely that these still suffer from adverse effects in the periplasm. None of them contain cysteines excluding promiscuous disulfide bond formation as a cause for their ineffective fluorescence. Chromophore maturation continues after fixation while protein folding stops. It is thus likely that the non-fluorescing FP fraction had not folded properly under periplasmic conditions. This is supported by the strong fluorescence signals from the periplasm of stationary living cells where protein folding could continue over time (Fig. S1).

Together, these results show that periplasmic conditions can be inhospitable for FPs regardless of their lack of cysteines and suggest that proper folding is the first prerequisite for periplasmic fluorescence. The use of co-translational transport for the periplasmic expression of FPs is a good method to select for well-folding variants and low-expression toxicity. mCherry is still the preferred periplasmic FP and FRET acceptor to mNG. Although no superior acceptor was found, the same tools could be employed to select for a high quantum yield donor FP to mNG as an acceptor. Indeed, mNG was shown to be an efficient acceptor to the cyan FP mTq2 with an R_0 value of 6.0 nm with FRET efficiencies in eukaryotes of 50–60% (Shaner *et al.*, 2013; Mastop *et al.*, 2017), making mTq2 a logical candidate to optimize for expression in the periplasm.

Superfolder mTq2 folds and matures in the periplasm

Aequorea victoria-derived FPs contain two cysteines, C48 and C70, and were therefore initially not tested. However, sfGFP folds and fluoresces in the periplasm of *E. coli* (Aronson *et al.*, 2011) despite the presence of cysteines (Pédelacq *et al.*, 2006). This observation further suggests that the folding rate may be more important than the presence of cysteines for optimal periplasmic chromophore development.

Bright cyan FPs are great FRET donors because of their high quantum yield (QY). mTurquoise2 (mTq2) has a QY of 93% and was shown to allow high FRET efficiencies with mNG (Goedhart *et al.*, 2012; Shaner *et al.*, 2013; Mastop *et al.*, 2017). It can be paired with green, yellow or orange acceptors that have a high molar extinction coefficient (ε) resulting in relatively high R_0 values and strong FRET pairs. mNG is the preferred FRET acceptor of mTq2 in eukaryotic cells with an R_0 of 6.0 nm and FRET efficiencies ranging up to 50–60% (Shaner *et al.*, 2013; Mastop *et al.*, 2017).

mTq2 was tested in the periplasm of *E. coli* but it did not fluoresce (Fig. 3A). Since mTq2 is also derived from *Aequorea victoria,* superfolding mutations S30R, Y39N, N105T F99S, and I171V (Fukuda *et al.*, 2000; Pédelacq *et al.*, 2006) were introduced based on sfGFP to create superfolder mTq2 (sfTq2). sfGFP mutations M153T and V163A were already in mTq2 and Y145F was not included since it is close to the chromophore and could affect maturation and indeed negatively impact periplasmic fluorescence (Fig. S3). A206V was not introduced since it may increase dimerization tendency (Cranfill *et al.*, 2016).

mTq2 and sfTq2 fusions were expressed in the periplasm of *E. coli* growing in a plate reader at a concentration range of the inducer IPTG (Experimental procedures). Cultures expressing either mTq2 or sfTq2 resulted in toxicity correlated with induction concentrations previously reported for other FPs (Meiresonne *et al.*, 2017). However, sfTq2 could be expressed at higher levels with less toxicity compared to mTq2. Strikingly, the sfTq2 fusion resulted in periplasmic fluorescence, whereas the mTq2 fusions did not (Fig. 3A). This shows that the superfolder mutations enable sfTq2, like sfGFP, to fold and mature in the periplasm.

Cells expressing mTq2 and sfTq2 in the periplasm at non-toxic concentrations were imaged by fluorescence microscopy. Quantification of the signals from living, fixed and fixed and matured samples showed periplasmic fluorescence of sfTq2 only (Fig. 3B and C). Western blot analysis confirmed the similar expression levels of mTq2 and sfTq2 (shown in the next section).

The sfTq2-mNG FRET pair in the periplasm

Superfolder mutations allowed sfTq2 to fold and mature in the periplasm. To show that the periplasmic emission of sfTq2 is unaltered compared to cytoplasmic emission, *E. coli* was grown to steady state in minimal medium at 28°C. Expression of the cytoplasmic sfTq2 or periplasmic OM-bound OmpA-sfTq2 was induced for at least 2 mass doublings (MDs) with 15 μM IPTG. The samples were fixed, washed with PBS, diluted to an OD_{450} value of 1.000 ± 0.002 and the fluorescence spectra were measured. The normalized emission spectra were almost identical for cytoplasmically or periplasmically expressed sfTq2 (Fig. 4A).

Next, we tested how the new donor performed in FRET experiments with mNG. Cytoplasmic mNG-sfTq2 was capable of high rates of energy transfer with Ef_A values of 64.5 ± 3.0% but the periplasmic mNG-sfTq2 tandem only reached 18.8 ± 2.1%. A technical negative control, consisting of non-interacting proteins between the IM and OM, yielded –0.3 ± 1.4% energy transfer. The previously described (Meiresonne *et al.*, 2017) biological homodimerization interaction of the active and inactive *D,D*-carboxypeptidase PBP5 was confirmed with Ef_A values of 4.2 ± 2.7% and 8.8 ± 4.2%, respectively (Fig. 4B and Table 1). Although the sfTq2-mNG FRET pair could be used successfully to measure periplasmic protein interactions, the discrepancy between the cytoplasmic and periplasmic rates of energy transfer indicated sfTq2 did not reach its full potential. For comparison, our mNG-mCh FRET assay allows the detection of the cytoplasmic and periplasmic protein interactions with more comparable Ef_A values up to 19 and 16%, respectively (Meiresonne *et al.*, 2017).

The periplasm is an oxidative environment and the presence of cysteines can cause the formation of non-fluorescent oligomers (Costantini *et al.*, 2015). The introduced superfolder mutations in sfTq2 may not necessarily fully protect its two native cysteines from promiscuous disulfide bridge formation in the periplasm. Therefore, we set out to replace the cysteines of sfTq2 by site-directed and random mutagenesis and tested the resulting FPs in the periplasm.

Development and optimization of sfTq2^{ox}

To improve the expression of sfTq2 in the periplasm, site-directed mutagenesis was performed to replace sfTq2's C48 with serine and C70 with serine, methionine or valine. Serine closely resembles cysteine with a hydroxyl instead of a sulfhydryl group. Methionine also contains a sulphur that is not nucleophilic and therefore

should not participate in disulfide bond formation. Valine should resemble the more hydrophobic state of cysteine better than serine and was shown to aid fluorescence of oxBFP in the eukaryotic ER (Costantini *et al.*, 2015).

Single and double cysteine mutants of sfTq2 performed better than sfTq2 in the periplasm with reduced toxicity and improved fluorescence (Figs 5 and S4). They were expressed as protein fusions in the periplasm of *E. coli* under non-toxic conditions and the fluorescence signals of living, fixed and fixed and matured samples were quantified. sfTq2 mutants C48S, C70S, C70V and C48S-C70V showed much brighter signals in the periplasm (Fig. 5B

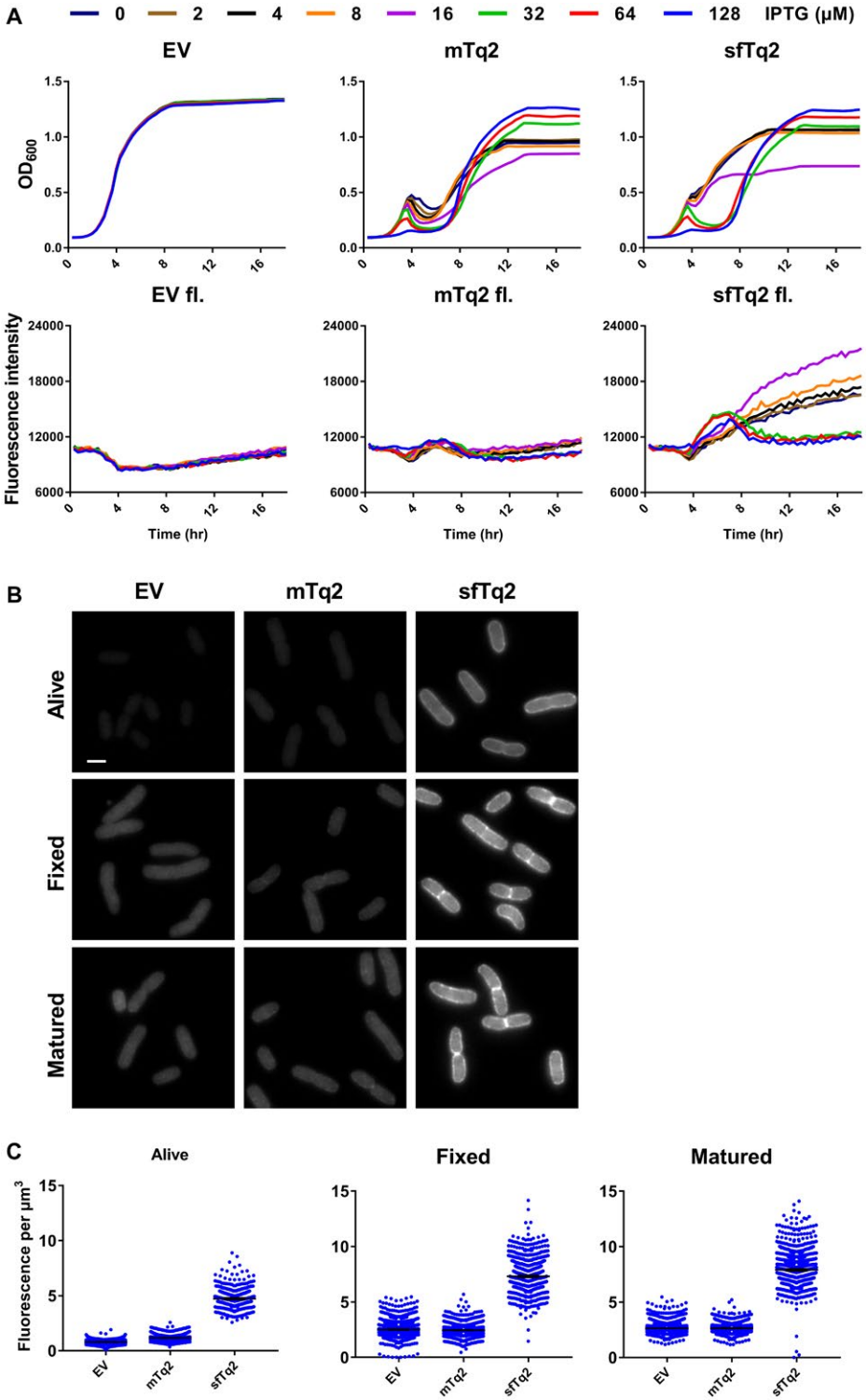

Fig. 3. Superfolder mTurquoise2 fluoresces in the periplasm.
A. Plate reader growth data in rich medium at 37°C show that the periplasmic sfTq2 expression is less toxic at high induction than the original mTq2. Plate reader fluorescence measurements confirm that periplasmic sfTq2 gives fluorescent signals while mTq2 does not.
B. Fluorescence microscopy of living cells expressing an empty vector control, mTq2-PBP5 or sfTq2-PBP5, reveals fluorescence only from the sfTq2 fusion. Fixation of the same cells does not result in a decreased sfTq2 signal. Overnight maturation of the fixed cells at RT to allow for possible chromophore (re)formation (indicated as 'matured') did not result in an increase in fluorescence for periplasmic mTq2 suggesting it had not folded properly while sfTq2 showed a strong periplasmic signal. All photographs are shown with the same grey values (100–4000) for comparison and the scale bar represents 2 μm.
C. Quantification of the control, mTq2 and sfTq2 cultures for the living, fixed and matured cells shows no difference between the empty vector control and the mTq2 cells. The sfTq2 cells showed a small maturation effect. The error bars at the mean represent the 95% confidence interval. The number of cells measured were: Alive) EV = 1018, mTq2 = 650 and sfTq2 = 571. Fixed) EV = 1176, mTq2 = 1046, sfTq2 = 884. Fixed and matured) EV = 1142, mTq2 = 931, sfTq2 = 988.

and C). The methionine sfTq2 variants did not perform better than sfTq2 in terms of fluorescence (Fig. S4). Western blotting showed that all cysteine replacement mutants were better expressed in the periplasm regardless of fluorescence signals (Fig. 5D). This is in line with the secretory improvement of GFP to the eukaryotic ER by cysteine replacements (Jain *et al.*, 2001). The enhanced periplasmic production but dim fluorescence of some sfTq2 variants suggests poor chromophore maturation.

Site-directed random mutagenesis of sfTq2 cysteines revealed that residue 48 does not allow much variation besides the original cysteine or serine while a variety of amino acids are accepted as residue 70. Several brightly fluorescing sfTq2 variants were found but none of them showed improved periplasmic fluorescence as compared to C70V (Supplementary text 1, Fig. S5). Cysteine mutants in the parental mTq2 did not increase periplasmic fluorescence, although a reduction in expression toxicity was observed (Fig. S6). sfGFP mutant sfGFP^{C70V} showed similar periplasmic fluorescence compared to its predecessor and expression was slightly less toxic (Fig. S7). This shows that cysteines are involved in translocation toxicity and subsequent low production of periplasmic fusion proteins.

All experiments showed that sfTq2^{C70V} was the best periplasmic variant to be used in the bacterial periplasm in terms of reduced toxicity, fluorescence intensity and fast folding or maturation. sfTq2^{C70V} was named sfTq2^{ox}. Subsequent comparisons of sfTq2 and sfTq2^{ox} as periplasmic fusions to several IM and OM localized proteins confirmed the superior performance of sfTq2^{ox} (Figs S8–S10).

The superior periplasmic properties of sfTq2^{ox} come without a trade-off

Introducing superfolder mutations in mTq2 allowed fluorescence in the periplasm of *E. coli*. The additional C70V

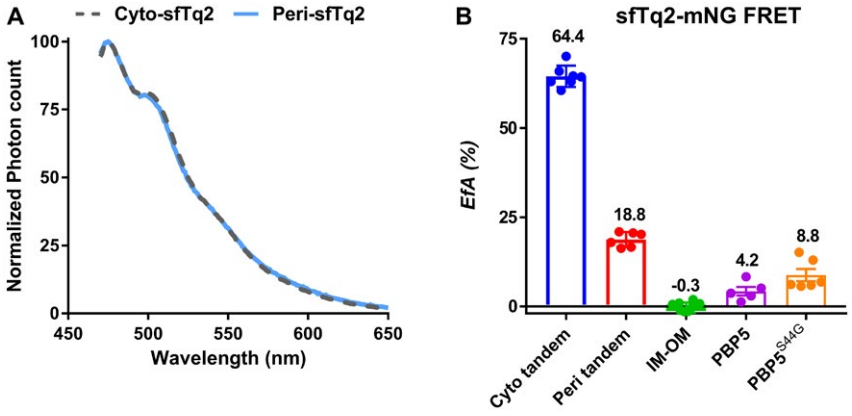

Fig. 4. *In vivo* FRET using the sfTq2-mNG FRET pair.
A. Periplasmic sfTq2 does not show altered spectra compared to cytoplasmic sfTq2. LMC500 grown to steady state in minimal medium at 28°C were induced to express sfTq2 freely in the cytoplasm or the periplasm as the OM-bound OmpA-sfTq2 fusion. After 2 MDs, the cells were fixed, washed with PBS and set to an OD_{450} value of 1.000 ± 0.002 before measuring the fluorescence spectra. The normalized fluorescence spectra show the same shape suggesting that the spectral properties of sfTq2 are the same in the cytoplasmic and periplasmic compartments.
B. Ef_A values calculated for the sfTq2-mNG FRET pair show a large difference for the cytoplasmic and periplasmic tandem. The technical negative control (IM-OM) did not show any energy transfer. The activity-related conformational changes of the PBP5 dimers previously observed with the mNG-mCh FRET pair (Meiresonne et al., 2017) were confirmed. The error bars represent the mean and standard deviation. The control Ef_A values were calculated from experiments in LMC500 and CS109 Δ*dacA* and the PBP5 dimerization experiments were exclusively performed in CS109 Δ*dacA*. Table S2 shows the FRET efficiencies measured with the plate reader. Representative unmixing data are shown in Fig. S14.

Table 1. FRET efficiencies obtained with mTq2 variants measured by fluorometry.

	Donor FP to mNG	Fusion position	Ef_A (%)	SD	Repeats
Cytoplasmic FRET					
Positive control tandems					
mNG-mTq2	mTq2	Free floating	61.3	6.4	4
mNG-sfTq2	sfTq2	Free floating	64.5	3.0	7
mNG-sfTq2^{C70V}	sfTq2^{ox}	Free floating	66.4	3.1	8
Periplasmic FRET					
Positive control tandems					
mNG-sfTq2	sfTq2	OmpA177 (OM)	18.8	2.1	6
mNG-sfTq2^{C48S}	C48S	OmpA177	32.9	1.9	2
mNG-sfTq2^{C70V}	sfTq2^{ox}	OmpA177	39.1	3.8	11
mNG-sfTq2$^{C48S-C70V}$	C48S-C70V	OmpA177	40.3	1.2	2
mNG-sfTq2^{C70V}	sfTq2^{ox}	OmpA177*	42.5	3.1	6
mNG-sfTq2^{C70V}	sfTq2^{ox}	LpoB73 (OM)	39.8	2.1	5
mNG-sfTq2^{C70V}	sfTq2^{ox}	NlpA^{ss} (IM)	41.2	2.4	7
mNG-sfTq2^{C70V}	sfTq2^{ox}	MalF^{ss-mss} (IM)	42.9	2.5	3
Negative controls					
mNG-sfTq2 (IM-OM)	sfTq2	PBP5, OmpA177	–1.4	1.4	4
mNG-sfTq2^{C70V} (IM-OM)	sfTq2^{ox}	PBP5, OmpA177	–1.3	2.2	13
mNG-sfTq2^{C70V} (IM, IM)	sfTq2^{ox}	NlpA^{ss}, FtsB	–0.7	1.7	10
Biological interactions					
PBP5 + PBP5	sfTq2	IM, IM	4.2	2.7	5
PBP5^{S44G} + PBP5^{S44G}	sfTq2	IM, IM	8.8	4.2	6
FtsB + FtsL	sfTq2^{ox}	IM, IM	19.2	4.5	8
FtsL + FtsB	sfTq2^{ox}	IM, IM	15.6	2.6	8
FtsL^{m4} + FtsB	sfTq2^{ox}	IM, IM	3.1	2.1	3
FtsL^{m4} + FtsB^{m4}	sfTq2^{ox}	IM, IM	3.0	3.4	3

SS, signal sequence; mss, membrane spanning sequence, LpoB73 indicates residue 1-73 of LpoB, OmpA177 indicates residue 1-177 of OmpA, * indicates a different linker between mNG and sfTq2^{ox} (EF instead of EL due to differences in cloning). Table S2 shows the FRET efficiencies for the new mTq2 variants measured with the plate reader. Representative unmixing data are shown in Fig. S14; the plate reader unmixing data are shown in Fig. S15.

mutation in sfTq2^{ox} resulted in a reduction in expression toxicity and the brightest periplasmic fluorescence. Interestingly, mTq2, sfTq2 and sfTq2^{ox} were equally bright when expressed in the cytoplasm (Fig. S11). To verify the *in vivo* spectroscopic properties of the mTq2 variants, the fluorescence lifetime and cellular brightness were determined.

The quantum yield of cyan FPs is directly related to their fluorescence lifetime (Goedhart *et al*., 2010; 2012). Therefore, the lifetimes of mTq2 and sfTq2 and sfTq2^{ox} were measured from the cytoplasm of eukaryotic (HeLa) cells using frequency domain fluorescence lifetime imaging microscopy (FLIM). This resulted in an identical distribution of lifetimes with an average of 3.9 ± 0.1 ns suggesting no differences in QY between the three variants (Fig. 6A). The fluorescence lifetime of sfTq2 and sfTq2^{ox} expressed in the periplasm also showed a similar average lifetime of 3.9 ± 0.1 ns showing that periplasmic conditions did not alter their lifetime and suggesting an unaltered QY (Fig. 6B). Agar colonies of *E. coli* expressing cytoplasmic mTq2, sfTq2 or sfTq2^{ox} were imaged and gave a similar average lifetime of 3.8 ± 0.2 ns (Fig. S11).

To analyse the cellular brightness of sfTq2 and sfTq2^{ox}, self-cleaving viral peptide (2A)-linked tandems with super yellow FP 2 (sYFP2) were expressed in HeLa cells (Mastop *et al*., 2017). The equal expression of both FPs (Kim *et al*., 2011) showed a similar correlation for the three mTq2 variants reflecting an equal cellular brightness (Fig. 6C). Quantification of mTq2, sfTq2 and sfTq2^{ox} expressed in the cytoplasm of *E. coli* further supports this (Figs 6D and S11).

Having determined that the lifetime and cellular brightness of sfTq2^{ox} are the same as that of mTq2 and sfTq2, it is reasonable to assume that the extinction coefficient is also similar. The unaltered lifetime also implies that the spectroscopic properties (quantum yield) of mTq2 may be used for calculating R_0 and the quantification of Ef_A values.

mTq2 is monomeric (Cranfill *et al*., 2016) and will therefore not obscure FRET experiments by dimerization or oligomerization. The superfolder and C70V mutations may have impacted this property. Therefore, the tendency of sfTq2 and sfTq2^{ox} to form undesired oligomers was assessed by the OSER assay (Costantini *et al*., 2012) showing equal results for both proteins, suggesting the same low propensity to aggregate as mTq2 (Fig. S12).

Further confirmation that sfTq2 and sfTq2^{ox} have the same spectral properties as mTq2 comes from their

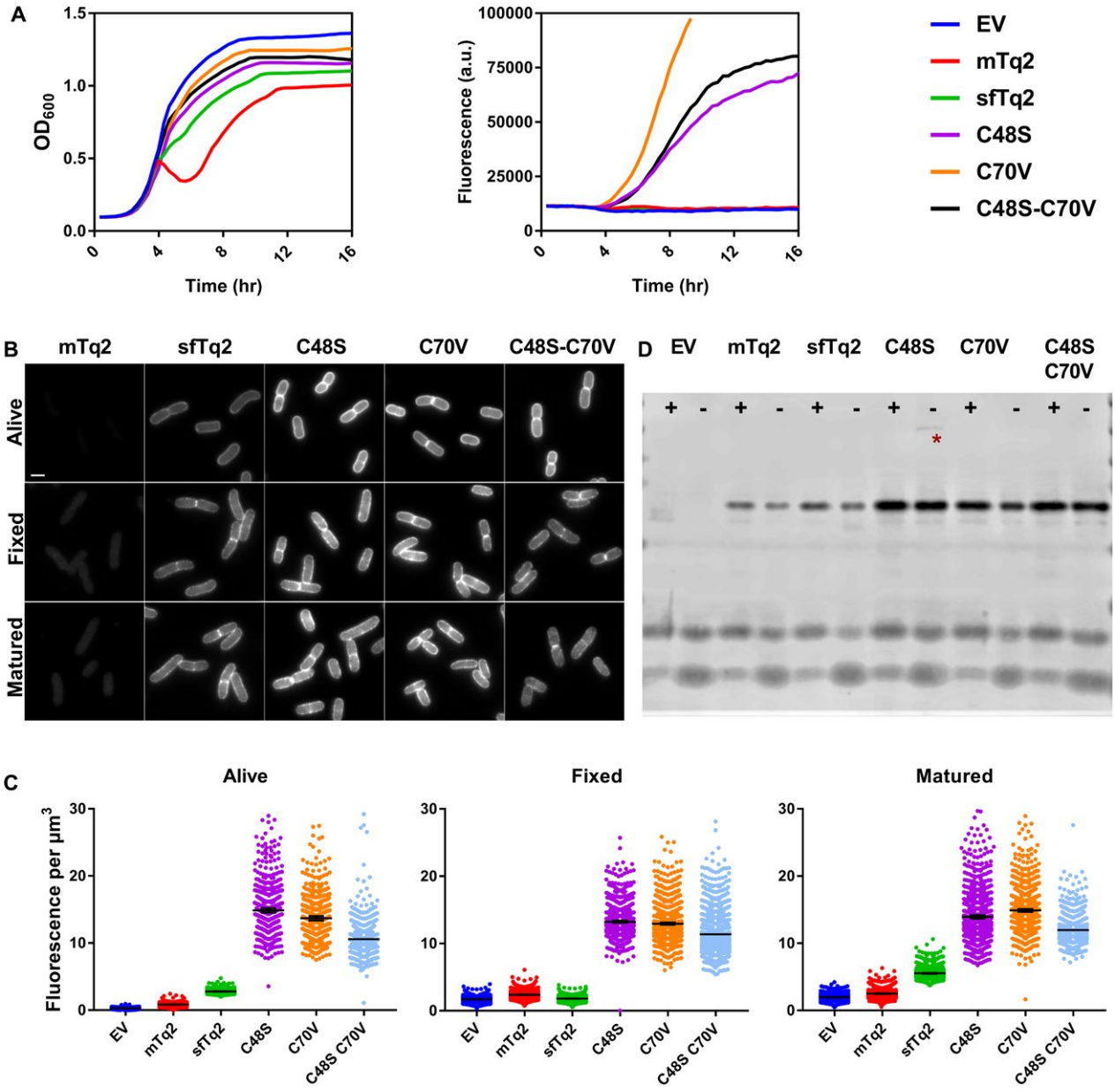

Fig. 5. Cysteine-replaced sfTq2 variants perform better in the periplasm.
A. Periplasmic expression of sfTq2-PBP5 variants in LMC500 grown in rich medium at 37°C at relatively non-toxic induction conditions results in large differences in cyan fluorescence. The C70V variant performs better than C48S and the double cysteine mutant version.
B. Microscopy of LMC500 grown in rich medium and induced with 15 µM IPTG shows strong fluorescence for the sfTq2-PBP5 variants in the periplasm. For comparison, the greyscale of all photographs are the same (80–7000) and the scale bar represents 2 µm.
C. Quantification of the images confirms bright fluorescence signals from the single C48S and C70V sfTq2 variants. Differences in fluorescence with the prolonged plate reader induction suggest that folding difficulties may still be a problem. The error bars at the mean represent the 95% confidence interval. The number of cells measured were between: Alive 500–1000, Fixed 1000–1500 and Matured 1000–2000 except for EV-Alive $n = 327$ and C48S-C70V-Fixed $n = 775$. D. mTq2 is produced at similar levels as sfTq2 but does not fold properly; cysteine mutants of sfTq2 are produced at higher levels. Anti-GFP immunoblotting of the corresponding samples shows that the fusion proteins are intact and that C48S has a minor propensity to form higher order complexes (asterisk). The + and signs, respectively, indicate the presence or absence of the reducing agent DTT in the sample.

FRET efficiencies in the cytoplasm. Tandem fusions of mNG with mTq2, sfTq2 or sfTq2^{ox} resulted in significantly similar Ef_A values of 61 ± 6%, 65 ± 3% and 66 ± 3%, respectively (Table 1). The same constructs expressed in agar colonies of *E. coli* gave an average lifetime of 2.5 ± 0.1 ns, a 35% reduction in fluorescence lifetime compared to their single donor FPs (Fig. S11). This is similar to the 33% energy transfer observed for mNG-mTq2

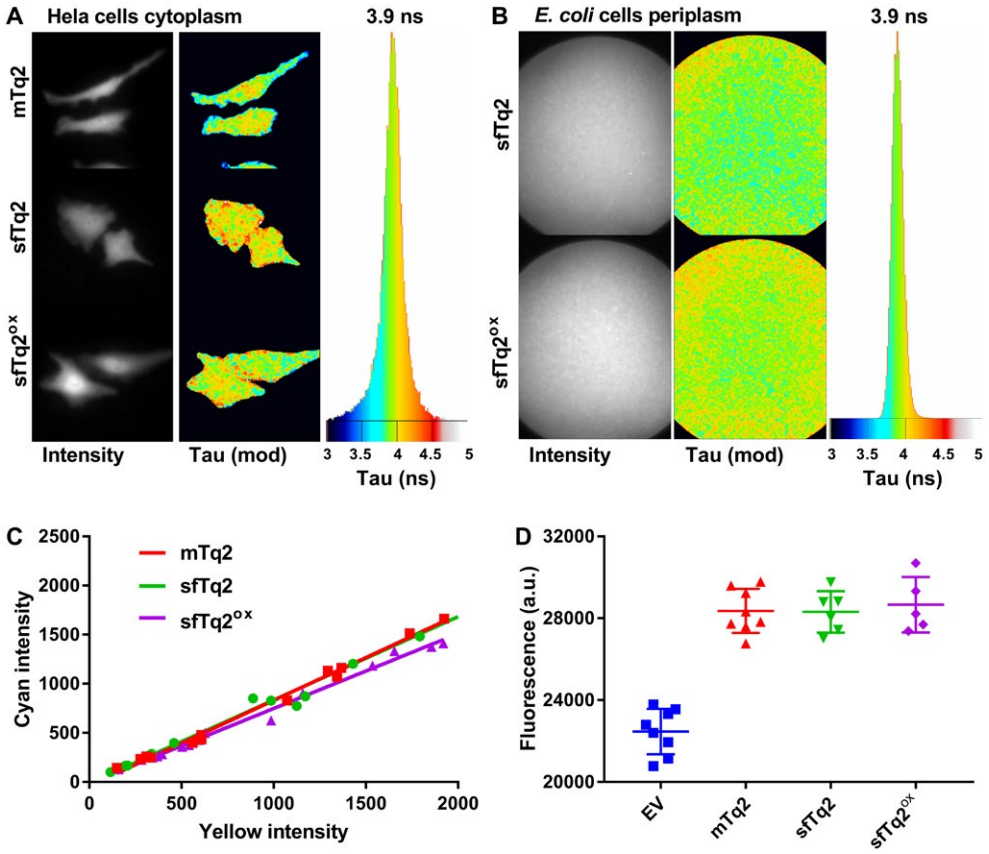

Fig. 6. sfTq2^{ox} comes without a trade-off.
A. Frequency domain FLIM of HeLa cells expressing mTq2, sfTq2 or sfTq2^{ox} in the cytoplasm reveals a similar average fluorescence lifetime of 3.9 ns.
B. FLIM of a suspension of *E. coli* cells expressing periplasmic OmpA-sfTq2 or OmpA-sfTq2^{ox} also show a similar fluorescence lifetime of 3.9 ns.
C. The cellular brightness of mTq2, sfTq2 and sfTq2^{ox} is equal in Hela cells. The slope coefficients of the fits are, respectively: 0.87, 0.84 and 0.76.
D. Fixed samples of LMC500 cells at OD_{450} = 1.00 expressing cytoplasmic mTq2, sfTq2 or sfTq2^{ox} show equal amounts of fluorescence.

in eukaryotic cells that were measured using the same technique (Mastop *et al.*, 2017).

Taken together, these results strongly indicate that the engineering of sfTq2^{ox} comes without a trade-off compared to its parent mTq2 with the added benefits of periplasmic expression, bright fluorescence and reduced toxicity.

High dynamic range periplasmic FRET with sfTq2^{ox}

mTq2 forms a good FRET pair with mNG with an R_0 of 6.0 nm. The cytoplasmic tandems of mTq2 and sfTq2 gave similar rates of energy transfer. Yet, the periplasmic mNG-sfTq2 tandem gave an Ef_A value of 18.8 ± 2.1% suggesting differences in terms of periplasmic functionality. The bright periplasmic fluorescence of cysteine-replaced sfTq2 variants suggested that they would make better donors to mNG for periplasmic FRET. mNG-sfTq2 tandems containing the cysteine mutants, associated with the OM through OmpA, were tested for their *in vivo* FRET efficiencies. This indeed greatly improved Ef_A values to 32.3 ± 1.9, 42.5 ± 3.1% and 40.3 ± 1.2% for sfTq2^{C48S}, sfTq2^{ox} or sfTq2$^{C48S-C70V}$, respectively. No degradation or cleavage products were detected by western blotting (Fig. S13).

Since sfTq2^{ox} showed the best periplasmic behaviour compared to all other cysteine mutant variants, mNG-sfTq2^{ox} fusions were made to other periplasmic proteins to exclude localization effects. Tandems were associated with the OM or IM through the translocation and lipidation signals of lipoproteins LpoB and NlpA, respectively. A third tandem was localized to the IM through the first membrane spanning sequence of MalF (Fig. 7). All periplasmic tandems resulted in Ef_A values of 40% (Table 1) suggesting that this is the highest attainable FRET efficiency for mNG-sfTq2^{ox} in the periplasm regardless the location of the fusion. Negative controls, assaying energy transfer by crowding conditions in the IM or between the IM and OM, resulted in Ef_A values of −0.7 ± 1.7% and −1.3 ± 2.2%, respectively (Fig. 7). All assayed Ef_A values are shown in Table 1. The measured FRET efficiencies were confirmed

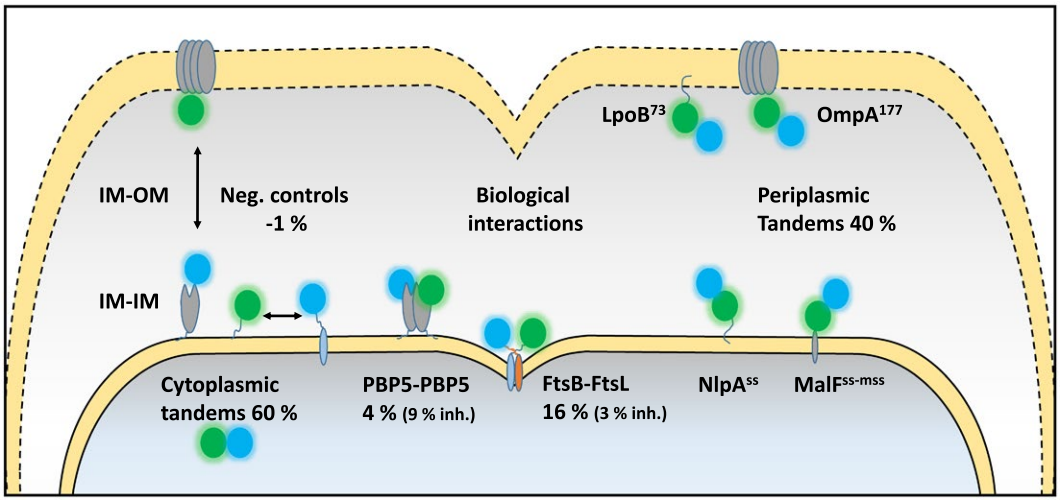

Fig. 7. Schematic overview showing the subcellular localization of the periplasmic protein interactions and controls assayed with the sfTq2^{ox}-mNG FRET pair. PBP5 dimerization interactions were assayed with sfTq2-mNG. Inh. refers to the inactive mutants PBP5^{S44G}, FtsB^{m4} and FtsL^{m4}. A full list of Ef_A values is shown in Table 1.

using a separate 96-wells plate reader set up showing that the throughput of FRET assays using the sfTq2^{ox}-mNG pair can be greatly increased (Table S2).

In vivo *interactions of putative antibiotic targets in the periplasm*

With the periplasmic sfTq2^{ox}-mNG FRET pair established, biological interactions could be assessed. The periplasm contains many relevant potential antibiotic targets including the cell division subcomplex of FtsB, FtsL and FtsQ (FtsBLQ) (den Blaauwen *et al.*, 2014). All three components are essential and are thought to form the regulating link between the cytoplasmic and periplasmic machineries of cell division (Liu *et al.*, 2015; Boes *et al.*, 2019). Assaying the interactions in this complex could allow for the screening of novel antibiotics *in vivo*, determining the efficacy and specificity at the same time. FRET experiments assaying the interaction between FtsB-sfTq2^{ox} and FtsL-mNG or FtsB-mNG and FtsL-sfTq2^{ox} resulted in Ef_A values of 19.2 ± 4.5% and 15.6 ± 2.6%, respectively (Table 1 and Fig. 7). A negative control for IM-associated proteins of FtsB-sfTq2^{ox} with NlpA^{ss}-mNG resulted in an Ef_A value of −0.7 ± 1.7%. FtsB and FtsL were reported to interact through a leucine zipper-like motif that can be disrupted by leucine to alanine substitutions (Robichon *et al.*, 2011). The leucine zipper mutants of FtsB, FtsB^{m4} and FtsL, FtsL^{m4} are good controls as they are able to localize at the division site and complement their respective depletion strains (Robichon *et al.*, 2011). The interactions of wild-type FtsB-mNG or mutant FtsB^{m4}-mNG with mutant FtsL^{m4}-sfTq2^{ox} showed decreased Ef_A values of 3.1 ± 2.1% and 3.0 ± 3.4%, respectively. Expression without degradation of wild-type and mutant FtsB and FtsL constructs was confirmed by western blotting (Fig. S13). The weakening of the leucine zipper motif clearly reduces the interaction between the two proteins given the decrease in Ef_A values. This observed reduced affinity between the two proteins may reflect a reduction in their average interaction time. In conclusion, the new FRET pair sfTq2^{ox}-mNG can be used to detect periplasmic protein interactions *in vivo* and paves the way for functional screening of essential antibiotic targets.

Discussion

In vivo visualization of periplasmic proteins by fusions to FPs is difficult since most do not fold or mature due to the oxidizing environment and the necessity of transport. Additionally, over-expressing periplasmic FP fusions can lead to toxicity and counter selection (Meiresonne *et al.*, 2017). The limited choice of FPs is especially problematic for applications that use multiple FPs, such as multiplex imaging and FRET studies. For FRET studies, a pair of FPs with a high R_0 is desired. The theoretical R_0 value, however, does not take into account the proper folding and maturation of FPs *in vivo*. Therefore, the optimal FP for specific conditions should be experimentally determined. We aimed to improve our previously developed periplasmic FRET assay using mNG-mCh (R_0 = 5.5 nm) by searching alternatives for mCherry, which has a modest quantum yield (QY) and subsequent brightness. However, testing bright cysteine-less red FPs showed

that mCherry is still the preferred FP in the periplasm due to its favourable folding and maturation properties.

mNG has a high QY and extinction coefficient and can therefore function as a donor or acceptor FP (Shaner *et al*., 2013). It forms an efficient FRET pair with mTq2 (R_0 = 6.0 nm) and allows for highly efficient energy transfer (Shaner *et al*., 2013; Mastop *et al*., 2017). Since mTq2 did not fluoresce in the periplasm, sfTq2 was engineered by introducing superfolder mutations S30R, Y39N, N105T F99S, M153T, V163A and I171V based on the related sfGFP, which is fluorescent in the periplasm (Aronson *et al*., 2011). sfTq2 was functional in the periplasm but allowed only moderate periplasmic FRET with mNG (Fig. 4 and Table 1).

The oxidative environment of the periplasm facilitates disulfide bond formation between exposed cysteines in close proximity (Aronson *et al*., 2011). *Aequorea victoria*-derived FPs are adapted for cytoplasmic conditions and their native cysteines are thus prone to promiscuous disulfide bonding in the periplasm resulting in non-fluorescent oligomers. Site-directed random mutagenesis of C48 and C70 in sfTq2 resulted in greatly increased periplasmic fluorescence and reduced expression toxicity with the single C70V variant (sfTq2^{ox}) giving the best results (Figs 5, S4, and S5). sfTq2^{ox} came without an observed trade-off as the same QY and brightness values were found for mTq2 and sfTq2 (Fig. 6). The development of sfTq2^{ox} shows that periplasmic fluorescence of FPs first depends on their efficient folding and then on the prevention of cysteine disulfide bond formation.

Employing the mNG-sfTq2^{ox} FRET pair in the periplasm resulted in energy transfer rates of 40% for periplasmic tandems (Fig. 7). FRET efficiencies of 60% were observed for cytoplasmic mTq2, sfTq2 or sfTq2^{ox} fusions to mNG (Table 1). Based on the R_0 value (6.0 nm), the FRET efficiency of 60 and 40% would correspond to a distance between the fluorophores of 5.6 and 6.4 nm, respectively. Both values are plausible given the minimal distance of ± 3 nm between the two chromophores of the FRET pair. Yet, it cannot be excluded that the transport to the periplasm still hampers subsequent folding of a fraction of the FPs resulting in a lower FRET efficiency.

A factor influencing FRET efficiency (and R_0 values) is the dipole orientation of the donor and acceptor chromophore. This would contribute to the FRET efficiency difference if the environment of the cytoplasm or the periplasm would restrict the rotational freedom of the tandem differently. Presently, no evidence is available to support such a difference. The comparison of mTq2 with several acceptor FPs shows that mNG is an exceptional FRET acceptor, even compared to FPs with similar spectroscopic properties (Mastop *et al*., 2017). Indeed, mNG is an outlier with its chordate origin compared to the usual cnidarian-derived FPs with different sequence homologies and possibly different behaviours (Shaner *et al*., 2013; Steiert *et al*., 2018).

Protein interactions often change significantly when the activity of one of the partners is inhibited by antibiotics (van der Ploeg *et al*., 2015). The Gram-negative periplasm facilitates a myriad of essential protein interactions waiting to be investigated *in vivo*. Using the new periplasmic FRET pair, we demonstrated the direct interaction and disruption of essential cell division proteins FtsB and FtsL with high rates of energy transfer. Interactions of the FtsBLQ complex are considered to be the link between the cytosolic and periplasmic parts of cell division setting off constriction (Liu *et al*., 2015; Boes *et al*., 2019). Exactly how and in what stoichiometry the complex forms and functions is still a matter of debate (Karimova *et al*., 2005; Villanelo *et al*., 2011; Robichon *et al*., 2011; Glas *et al*., 2015; Condon *et al*., 2018). Interactions between FtsB and FtsL seem to rely on their coiled-coil transmembrane helices (Robichon *et al*., 2011; Condon *et al*., 2018) while the interaction of FtsQ and FtsB requires their periplasmic soluble domains and forms independently of FtsL (van den Berg van Saparoea *et al*., 2013; Glas *et al*., 2015; Kureisaite-Ciziene *et al*., 2018; Choi *et al*., 2018; Boes *et al*., 2019). Our findings confirm the former interaction *in vivo* and provide a tool for the further dissection of FtsBLQ interactions.

The ability of FPs to fold and mature under non-native conditions is a property of increasing interest. Co-translational expression of fusion proteins in the periplasm is a good assay to select for optimized FPs. With the development of sfTq2^{ox}, the palette of periplasmic functional FPs is broadened to include members emitting at cyan wavelengths. This allows for the *in vivo* observation of (at least) three colours of periplasmic fusion proteins. Moreover, sfTq2^{ox} forms a FRET pair with mNG that can detect periplasmic protein interactions *in vivo* at double the detection range of previous bacterial FRET assays. mNG-sfTq2^{ox} is therefore the preferred FRET pair for the detection of periplasmic as well as cytoplasmic protein interactions paving the way for the screening of novel antibiotics that may inhibit them.

Experimental procedures

Bacterial strains and culturing conditions

The *Escherichia coli* K12 strains used are presented in (Table 2). The cells were cultured in rich medium (TY: 10 g Tryptone (Bacto laboratories, Australia), 5 g yeast extract (Duchefa, Amsterdam, The Netherlands) and 5 g NaCl (Merck, Kenilworth, NJ) per litre) supplemented with 0.5% glucose (Merck) or in glucose minimal medium (Gb1: 6.33 g K_2HPO_4 (Merck), 2.95 g KH_2PO_4 (Riedel de Haen, Seelze, Germany), 1.05 g $(NH_4)_2SO_4$ (Sigma, St. Louis, MO),

Table 2. Strains used in this study

Strain	Relevant characteristics	References
DH5α	F-, supE44, hsdR17, recA1, endA1, gyrA96, thi1, relA1	Bethesda Research Laboratories (1986)
LMC500	MC4100, F-, araD139, Δ(argF-lac)U169, deoC1, flbB5301, lysA1, ptsF25, rbsR, relA1, rpsL150	Taschner *et al.* (1988)
CS12-7	CS109 Δ*dacA*	Denome *et al.* (1999)

0.10 g $MgSO_4 \cdot 7H_2O$ (Roth, Karlsruhe, Germany), 0.28 mg $FeSO_4 \cdot 7H_2O$ (Sigma), 7.1 mg $Ca(NO_3)_2 \cdot 4H_2O$ (Sigma), 4 mg thiamine (Sigma), and 4 g glucose per litre, pH 7.0) at 28°C while shaking at 205 rpm. For growth in Gb1 of LMC500- and CS109-based strains, 50 mg/l lysine (Sigma) was added. Growth in rich and poor medium was at 37 and 28°C, respectively. Expression of constructs was induced with 15 μM isopropyl β-D-1-thiogalactopyranoside (IPTG, Promega, Madison, WI) unless stated otherwise. Plasmids were maintained in the strains by addition of 100 μg/ml ampicillin (Sigma) or 25 μg/ml chloramphenicol (Sigma). Growth was measured by absorbance at 600 or 450 nm with a Biochrom Libra S70 spectrophotometer (Harvard Biosciences, Holliston, MA) for TY or Gb1 cultures, respectively. Fixation was done with a final concentration of 2.8% formaldehyde and 0.04% glutaraldehyde in the shaking water bath for 15 min, after which the cells were harvested. After fixation, the cells were washed three times with 1 ml PBS.

Plasmid construction

An overview of the plasmids used in this study and their cloning strategies are given in Table S3. The sfTq2 nucleotide sequence (encoding mTurquoise2 with S30R, Y39N, F99S, N105T and I171V) was obtained by gene synthesis (MWG biotech). New constructs were created by restriction ligation cloning or site-directed mutagenesis. Inserted fragments were amplified by PCR from plasmid or the *E. coli* (LMC500) chromosome template, purified and restricted. For mutagenesis, a whole plasmid template was amplified by PCR using primers that contain the desired mutation. The resulting product was treated with *DpnI* to digest the methylated template plasmid. All restriction enzymes used were purchased from New England Biolabs Inc. (Ipswich, MA). For all PCR amplifications for cloning, the high-fidelity polymerase *pfux*7 was used (Nørholm, 2010) as per the manufacturer's instructions. An overview of the used primers is shown in Table S4.

Imaging and image analysis

For imaging the cells were immobilized on 1% agarose in water slabs on object glasses as described (Koppelman *et al.*, 2004) and photographed with a Hamamatsu ORCA-Flash-4.0LT (Hamamatsu, Naka-ku, Japan) CMOS camera mounted on an Olympus BX-60 fluorescence microscope (Tokyo, Japan) through a UPlanApo 100×/N.A. 1.35 oil Iris Ph3 objective. Images were acquired using the Micro Manager 1.4 plugin for ImageJ (Edelstein *et al.*, 2010). In all experiments, the cells were first photographed in phase contrast mode and then in fluorescence mode. The fluorescence filter cubes used were: U-MNG (red and orange, ex560/40, dic585LP, em630/75), EN-GFP (green, ex470/40, dic495LP, em525/50) and Cyan-GFPv2 (cyan, ex436/20, dic455LP, em480/40). Fluorescence backgrounds were subtracted using the modal values from the fluorescence images. Quantifications of cellular fluorescence were done using the ObjectJ plug-in of ImageJ (Vischer *et al.*, 2015). Living cells were imaged directly from the growing cultures and fixed cells directly after fixation and PBS washing. After fixation, the samples were allowed to mature overnight at RT, washed once more with 1 ml PBS and were then imaged. These samples are indicated in the text as 'matured'.

Western blot analysis

Samples for SDS–polyacrylamide gel electrophoresis and western blotting were prepared by pelleting live cells and equalizing biomass in MilliQ and subsequent boiling (95°C) in a sample buffer (0.0625 M Tris-Hcl pH 6.8, SDS 2%, glycerol 10%, bromphenol blue 0.001%) with and without dithiothreitol (0.1 M) reducing agent. Samples were loaded on 10% SDS-PAGE gels (stacking buffer (0.5 M Tris-HCl pH 6.8, 0.4% SDS), separating buffer (1.5 M Tris-HCl pH 8.7, 0.4% SDS), separated by electrophoresis and transferred onto a nitrocellulose membrane (Biorad) by wet blotting; bound antibodies were detected with the Odyssey FC scanner (LI-COR). The used antibodies were polyclonal rabbit α-GFP (1:2,000, Fisher Scientific) and polyclonal goat α-rabbit IRDye® 680LT (1:20,000, LI-COR).

FRET experiments and spectral measurements

FRET experiments were performed as described in (Meiresonne *et al.*, 2018) with modifications for the sfTq2-mNG FRET pair. Acceptor and donor emission spectra were collected with a fluorometer (Photon Technology International, NJ) through 6 nm slit widths with 1 s integration time per scanned nm and three times averaging. For the acceptor (mNG) channel, samples were excited by the monochromator set at 504 nm through a 500 ± 10 nm single band pass (BP) filter (BrightLine, Semrock, Rochester, NY) and emission wavelengths from 512 to 650 nm at 1 nm increments were measured through a 510 nm long-pass (LP) filter (Chroma technology corp., Bellow falls, VT). This spectrum was used to determine the amount of mNG in the sample. For the donor (mTq2, sfTq2 or $sfTq2^{ox}$) channel, samples were excited by the monochromator set at 450 nm through a 435 ± 40 nm BP filter (Semrock) and emission wavelengths from 470 to 650 nm at 1 nm increments were

collected through a 458 nm LP filter (Semrock). Knowing the amount of mNG present in the sample and the shape of the mNG and mTq2 variant reference spectra and background fluorescence spectrum in the cells, the sample spectra were unmixed into their separate components: background fluorescence, mTq2, mNG and sensitized emission (FRET). The FRET efficiencies were calculated using the published algorithms (Alexeeva *et al.*, 2010; Meiresonne *et al.*, 2018), using the spectral properties of mTq2 and mNG (Goedhart *et al.*, 2012; Shaner *et al.*, 2013). Spectral measurements using a multimode plate reader (BIOTEK Synergy MX, BioTek Instruments Inc., Winooski, VT) were performed as described (Meiresonne *et al.*, 2017; 2018) with the mTq2 variant donor channel acquisition set at 450 nm and emission scanning from 470 to 650 nm with minimal slit widths of 9 nm.

Frequency domain fluorescence lifetime measurements

FLIM experiments were essentially performed as described before (Goedhart *et al.*, 2012). For periplasmic samples in the solution, the exposure time was 500 ms, and the number of phase steps 18.

OSER assay

The OSER assay uses an ER localization sequence (CytERM) that was inserted in the multiple cloning site of pmTurquoise2-N1 to obtain CytERM-mTurquoise2 (Addgene plasmid Plasmid #98833). The coding sequence of mTurquoise2 was replaced by the superfolder variants. After transfection of the plasmids, the localization of the fusion was visualized by confocal microscopy. The OSER assay was performed as described before (Costantini *et al.*, 2012).

Molecular brightness assay

The cellular brightness assay was performed in HeLa cells as described before (Mastop *et al.*, 2017).

Author contributions

N.Y.M. and T.D.B. designed the study. N.Y.M., E.C., L.M.Y.M., J.G. and A.C. conducted the experiments and analysed the data. N.Y.M. and T.d.B. wrote the paper. All authors contributed to the final version of the manuscript.

Conflict of interest

The authors declare no competing financial interests.

Data availability

Mammalian plasmids sfTq2^{ox}-N1, sfTq2-N1 and sfTq2-C1 are available at Addgene: 117930, 117931 and 117932. Periplasmic expression plasmids sfTq2-PBP5 and sfTq2^{ox}-PBP5 are available at Addgene: 117959 and 117960.

Acknowledgements

We thank Eva Asmus and Alejandro Mónton Silva (University of Amsterdam, the Netherlands) for help with the experiments. Plasmids pCR119 and pCR124 were kind gifts from Daniel Ladant (Institut Pasteur, France). mScarlet-C1, mScarletI-C1 and mScarletH-C1 were kind gifts from Theodorus W.J. Gadella Jr. (University of Amsterdam, the Netherlands). N.Y.M. was supported by the NWO, ALW open program (82202019) and HFSP Program RGP0034/2013. E.C. and L.M.Y.M. were supported by the European Union's Horizon 2020 research and innovation programme under grant agreement No. 721484 (Train2Target).

References

Alexeeva, S., Gadella, T.W.J., Verheul, J., Verhoeven, G.S. and den Blaauwen, T. (2010) Direct interactions of early and late assembling division proteins in *Escherichia coli* cells resolved by FRET. *Molecular Microbiology*, **77**, 384–398.

Aronson, D.E., Costantini, L.M. and Snapp, E.L. (2011) Superfolder GFP is fluorescent in oxidizing environments when targeted via the Sec translocon. *Traffic*, **12**, 543–548.

Bethesda Research Laboratories. (1986) *E. coli* DH5 alpha competent cells. *Focus (Bethesda Research Laboratories)*, **8**, 9.

den Blaauwen, T., Andreu, J.M. and Monasterio, O. (2014) Bacterial cell division proteins as antibiotic targets. *Bioorganic Chemistry*, **55**, 27–38.

Boes, A., Breukink, E. and Terrak, M. (2019). Regulation of the peptidoglycan polymerase activity of PBP1b by antagonist. *mBio*, **10**, e01912–18.

Choi, Y., Kim, J., Yoon, H.-J., Jin, K.S., Ryu, S. and Lee, H.H. (2018) Structural insights into the FtsQ/FtsB/FtsL complex, a key component of the divisome. *Scientific Reports*, **8**, 18061.

Condon, S.G.F., Mahbuba, D.-A., Armstrong, C.R., Díaz-Vázquez, G., Craven, S.J., LaPointe, L.M., *et al.* (2018) The FtsLB subcomplex of the bacterial divisome is a tetramer with an uninterrupted FtsL helix linking the transmembrane and periplasmic regions. *Journal of Biological Chemistry*, **293**, 1623–1641.

Costantini, L.M., Fossati, M., Francolini, M. and Snapp, E.L. (2012) Assessing the tendency of fluorescent proteins to oligomerize under physiologic conditions. *Traffic*, **13**, 643–649.

Costantini, L.M., Baloban, M., Markwardt, M.L., Rizzo, M., Guo, F., Verkhusha, V.V., et al. (2015) A palette of fluorescent proteins optimized for diverse cellular environments. *Nature Communications*, **6**, 7670.

Cranfill, P.J., Sell, B.R., Baird, M.A., Allen, J.R., Lavagnino, Z., de Gruiter, H.M., et al. (2016) Quantitative assessment of fluorescent proteins. *Nature Methods*, **13**, 557–562.

Denome, S.A., Elf, P.K., Henderson, T.A., Nelson, D.E. and Young, K.D. (1999) *Escherichia coli* mutants lacking all possible combinations of eight penicillin binding proteins: viability, characteristics, and implications for peptidoglycan synthesis. *Journal of Bacteriology*, **181**, 3981–3993.

Edelstein, A., Amodaj, N., Hoover, K., Vale, R. and Stuurman, N. (2010) Computer control of microscopes using μManager. *Current Protocols in Molecular Biology*, Chapter 14, Unit14.20.

Fukuda, H., Arai, M. and Kuwajima, K. (2000) Folding of green fluorescent protein and the cycle3 mutant. *Biochemistry*, **39**, 12025–12032.

Glas, M., Van Den Berg, Bart, Van Saparoea, H., McLaughlin, S.H., Roseboom, W., Liu, F., *et al*. (2015) The soluble periplasmic domains of *Escherichia coli* cell division proteins FtsQ/FtsB/FtsL form a trimeric complex with submicromolar affinity. *Journal of Biological Chemistry*, **290**, 21498–21509.

Goedhart, J., Weeren, L.Van, Hink, M.A., Vischer, N.O.E., Jalink, K. and Gadella, T.W.J. (2010) Bright cyan fluorescent protein variants identified by fluorescence lifetime screening. *Nature Methods*, **7**, 137–139.

Goedhart, J., von Stetten, D., Noirclerc-Savoye, M., Lelimousin, M., Joosen, L., Hink, M.A., et al. (2012) Structure-guided evolution of cyan fluorescent proteins towards a quantum yield of 93%. *Nature Communications*, **3**, 751.

Harvey, B.R., Georgiou, G., Hayhurst, A., Jeong, K.J., Iverson, B.L. and Rogers, G.K. (2004) Anchored periplasmic expression, a versatile technology for the isolation of high-affinity antibodies from *Escherichia coli*-expressed libraries. *Proceedings of the National Academy of Sciences*, **101**, 9193–9198.

Jain, R.K., Joyce, P.B., Molinete, M., Halban, P.A. and Gorr, S.U. (2001) Oligomerization of green fluorescent protein in the secretory pathway of endocrine cells. *The Biochemical Journal*, **360**, 645–649.

Karimova, G., Dautin, N. and Ladant, D. (2005) Interaction network among *Escherichia coli* membrane proteins involved in cell division as revealed by bacterial two-hybrid analysis. *Journal of Bacteriology*, **187**, 2233–2243.

Kim, J.H., Lee, S.-R., Li, L.-H., Park, H.-J., Park, J.-H., Lee, K.Y., et al. (2011) High cleavage efficiency of a 2A peptide derived from porcine teschovirus-1 in human cell lines, Zebrafish and Mice. *PLoS ONE*, **6**, e18556.

Koppelman, C.-M., Aarsman, M.E.G., Postmus, J., Pas, E., Muijsers, A.O., Scheffers, D.-J., et al. (2004) R174 of *Escherichia coli* FtsZ is involved in membrane interaction and protofilament bundling, and is essential for cell division. *Molecular Microbiology*, **51**, 645–657.

Kureisaite-Ciziene, D., Varadajan, A., McLaughlin, S.H., Glas, M., Montón Silva, A., Luirink, R., et al. (2018) Structural analysis of the interaction between the bacterial cell division proteins FtsQ and FtsB. *mBio*, **9**(5), 321.

Liu, B., Persons, L., Lee, L. and de Boer, P.A.J. (2015) Roles for both FtsA and the FtsBLQ subcomplex in FtsN-stimulated cell constriction in *Escherichia coli*. *Molecular Microbiology*, **95**, 945–970.

Mastop, M., Bindels, D.S., Shaner, N.C., Postma, M., Gadella, T.W.J. and Goedhart, J. (2017) Characterization of a spectrally diverse set of fluorescent proteins as FRET acceptors for mTurquoise2. *Scientific Reports*, **7**, 11999.

Meiresonne, N.Y., van der Ploeg, R., Hink, M.A. and den Blaauwen, T. (2017) Activity-related conformational changes in D, D-carboxypeptidases revealed by in vivo periplasmic förster resonance energy transfer assay in escherichia coli. *mBio*, **8**, e01089-17.

Meiresonne, N., Alexeeva, S., van der Ploeg, R. and den Blaauwen, T. (2018) Detection of protein interactions in the cytoplasm and periplasm of Escherichia coli by Förster resonance energy transfer. *Bio-Protocol*, **7**, 1–24.

Nørholm, M.H. (2010) A mutant Pfu DNA polymerase designed for advanced uracil-excision DNA engineering. *BMC Biotechnology*, **10**, 21.

Pédelacq, J.-D., Cabantous, S., Tran, T., Terwilliger, T.C. and Waldo, G.S. (2006) Engineering and characterization of a superfolder green fluorescent protein. *Nature Biotechnology*, **24**, 79–88.

Piston, D.W.D.W. and Kremers, G.-J.G.J. (2007) Fluorescent protein FRET: the good, the bad and the ugly. *Trends in Biochemical Sciences*, **32**, 407–414.

van der Ploeg, R., Goudelis, S.T. and den Blaauwen, T. (2015) Validation of FRET assay for the screening of growth inhibitors of *Escherichia coli* reveals elongasome assembly dynamics. *International Journal of Molecular Sciences*, **16**, 17637–17654.

Robichon, C., Karimova, G., Beckwith, J. and Ladant, D. (2011) Role of leucine zipper motifs in association of the *Escherichia coli* cell division proteins FtsL and FtsB. *Journal of Bacteriology*, **193**, 4988–4992.

Shaner, N.C., Lambert, G.G., Chammas, A., Ni, Y., Cranfill, P.J., Baird, M.A., et al. (2013) A bright monomeric green fluorescent protein derived from *Branchiostoma lanceolatum*. *Nature Methods*, **10**, 407–409.

Steiert, F., Petrov, E.P., Schultz, P., Schwille, P. and Weidemann, T. (2018) Photophysical behavior of mNeonGreen, an evolutionarily distant green fluorescent protein. *Biophysical Journal*, **114**, 2419–2431.

Taschner, P.E., Huls, P.G., Pas, E. and Woldringh, C.L. (1988) Division behavior and shape changes in isogenic ftsZ, ftsQ, ftsA, pbpB, and ftsE cell division mutants of Escherichia coli during temperature shift experiments. *Journal of Bacteriology*, **170**, 1533–1540.

van den Berg van Saparoea, H., Glas, M., Vernooij, I.G.W.H., Bitter, W., Blaauwen, T.D. and Luirink, J. (2013) Fine-mapping the contact sites of the *Escherichia coli* cell division proteins FtsB and FtsL on the FtsQ protein. *Journal of Biological Chemistry*, **288**, 24340–24350.

Villanelo, F., Ordenes, A., Brunet, J., Lagos, R. and Monasterio, O. (2011) A model for the *Escherichia coli* FtsB/FtsL/FtsQ cell division complex. *BMC Structural Biology*, **11**, 28.

Vischer, N.O.E., Verheul, J., Postma, M., van den Berg van Saparoea, B., Galli, E., Natale, P., et al. (2015) Cell age dependent concentration of *Escherichia coli* divisome proteins analyzed with ImageJ and ObjectJ. *Frontiers in Microbiology*, **6**, 586.

Weiner, J.H. and Li, L. (2008) Proteome of the *Escherichia coli* envelope and technological challenges in membrane proteome analysis. *Biochimica et Biophysica Acta*, **1778**, 1698–1713.

Supporting Information

Additional supporting information may be found online in the Supporting Information section at the end of the article